# Mechanism of ultrafast modulation of the refraction index in photoexcited $In_xGa_{1-x}As/AlAs_ySb_{1-y}$ quantum well waveguides

G. W. Cong, R. Akimoto,* M. Nagase, T. Mozume, T. Hasama, and H. Ishikawa
*Ultrafast Photonic Devices Laboratory, National Institute of Advanced Industrial Science and Technology (AIST), AIST Tsukuba Central 2-1, Umezono 1-1-1, Tsukuba, Ibaraki 305-8568, Japan*
(Received 19 June 2008; published 6 August 2008)

Ultrafast index change induced by intersubband excitation in $In_xGa_{1-x}As/AlAs_ySb_{1-y}$ quantum well waveguides was evaluated by measuring the phase shift $\Delta\phi$ in a wide spectral range of 1.2–1.7 $\mu$m based on a spectral analysis. We obtained a large enhancement in $\Delta\phi$ by tuning the probe photon energy to interband absorption edge. The measured induced absorption $\Delta A$ also increased with reduction in the wavelength. The spectra of $\Delta\phi$ and $\Delta A$ were well explained by the interband dispersion model under intersubband excitation while the intersubband plasma dispersion previously reported has a negligible contribution.

DOI: 10.1103/PhysRevB.78.075308 PACS number(s): 78.67.De, 42.50.Ct, 73.21.Fg

The ability to modulate the refractive index has enabled us to adjust the group velocity of light, which is of particular interest for a broad range of phenomena such as stopping and storing optical pulses all optically,[1] photonic transitions,[2] gain without inversion,[3] and cross phase modulation (XPM).[4] Such all-optical light control is almost the ultimate goal of modern photonics.[5] Index modulation can be achieved by optical cavities[1,2] or strong light-matter interactions in quantum wells (QWs).[3] Intersubband transition (ISBT) in QWs has large optical nonlinearity and picosecond carrier relaxation; therefore, it is exciting if we can control the index of quantum wells by an all-optical means because this may stimulate functional devices based on advantages of QWs. Usually, the ISBT induced index change is effective for light with the same polarization mode as control light. For example, when we excite an ISBT by transverse-magnetic (TM) light, the index change, as well as the absorption, will happen in correspondence to this individual transition.[6] However, transverse-electric (TE) light that is inactive to ISBT is found to experience an index modulation of picosecond response under intersubband excitation in our $In_xGa_{1-x}As/AlAs_ySb_{1-y}$ coupled double quantum well (CDQW) waveguides.[7,8] An interferometric ultrafast all-optical switch based on this index modulation is promising in obtaining a lossless on state if a $\pi$-rad phase shift is achieved under a practical power level.[5,8] Therefore, compared with the switch based on TM light intensity modulation,[9] this interferometric switch will have high figure of merit due to the use of TE light that is free from intersubband absorption. The mechanism driving this cross-nature ultrafast index change is still not understood thoroughly due to the lack of experimental evaluation of the index change.[10] It is meaningful to clarify the mechanism not only for enhancing the power efficiency of phase shift but also for understanding the physics of nonlinear index response of QWs under intersubband excitation.

In this paper, the index change was evaluated by measuring the phase shift based on a spectral analysis method and we examine the photon energy dependence of ultrafast index modulation in QW system. We demonstrated a great enhancement of the phase shift by tuning the photon energy to interband absorption edge. A model based on intersubband-excitation enhanced interband transition well explained this ultrafast cross-nature index change. This mechanism in modulating refractive index of QWs has profound implications for optical communications and nonlinear optics.

Two possible origins may contribute to this XPM. One is the intersubband plasma model where the phase shift is attributed to the change in the total refractive index from the carrier plasma dispersion summed up from each subband due to the subband nonparabolicity and carrier redistribution.[11] The phase shift in this model is independent of the probe wavelength. The other is the interband dispersion model where the enhanced interband transition (IBT) (Refs. 12–14) takes place around the Fermi edge when the intersubband excitation partially depletes the carriers at the first subband. The index change will also occur although it was not studied in these works. When the photon energy approaches the interband absorption edge, the index change will greatly increase and so will the phase shift; this is contrary to the plasma model. With respect to this wavelength dependence, this model was not fully considered in Ref. 11. Furthermore, this model is effective for both heavy-hole (hh)-like and light-hole (lh)-like valence bands so that both TE and TM lights will undergo phase modulation. However, Drude model in two-dimensional systems is only effective for TE light owing to the in-plane electron excitation.[11] Therefore, we clarified the mechanism by examining the wavelength dependence of XPM for two samples having different IBT energies.

Two high-mesa waveguides (WGs) (S1 and S2) were fabricated into 3-$\mu$m-wide stripes of ~250 $\mu$m length. Their epitaxial layers can be respectively referred to in Refs. 15 and 8. The $In_xGa_{1-x}As/AlAs_ySb_{1-y}$ CDQW structures are shown in Fig. 1(a) with the self-consistently calculated results:[16] $x=0.53$ and 0.8, respectively, for S1 and S2, and $y=0.56$ for both. This calculation gives a good prediction in ISBT energies compared to the intersubband absorption spectra described elsewhere.[8,15] All layers other than the well layers in S2 and AlAs layers in both samples are lattice matched to InP substrate. The doping density in S1 and S2 are about $9\times10^{18}$ and $1.4\times10^{19}$ $cm^{-3}$, respectively. The interband absorption spectrum shows that the absorption edge in S1 is about 60 meV lower than that in S2, which depends

 

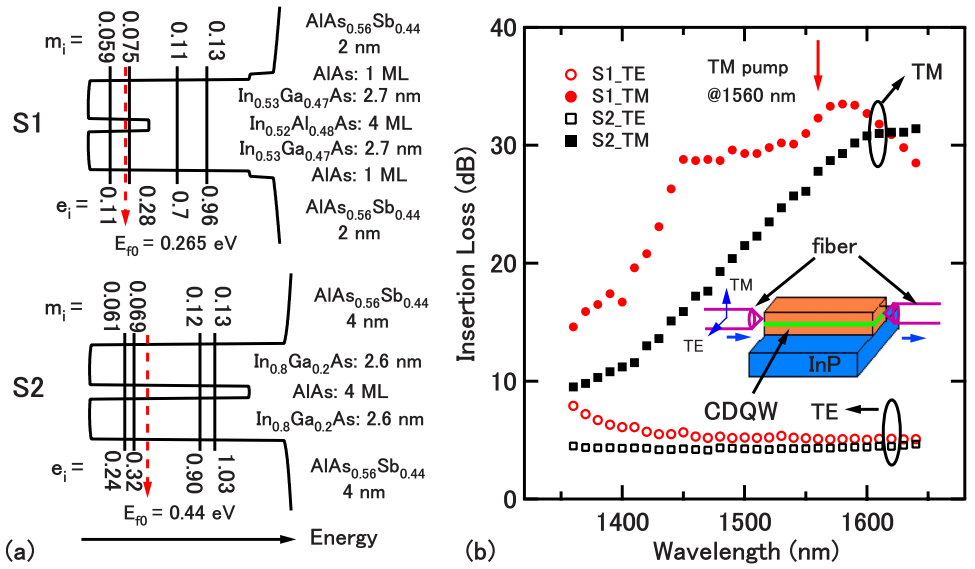


FIG. 1. (Color online) (a) CDQW structures with the electron mass ($m_i$ in $m_0$) and the sublevel energy ($e_i$ in electron volts) obtained by self-consistent Schrödinger-Poisson calculation including exchange-correlation and nonparabolicity effect. Red (dark gray) dashed lines show the steady-state Fermi energies $E_{f0}$. The reference level is the conduction-band edge in the well layer under flatband condition. (b) Waveguide insertion losses. Inset: waveguide-fiber alignment. The pump wavelength $\lambda_1$=1560 nm, which excites the $e_1$-$e_4$ transition.

on the valence-band dispersion, conduction-band nonparabolicity, and carrier density. In Fig. 1(b), the TE loss of S1 increases faster than that in S2 with the shortening of the wavelength, which supports that S1 has a smaller IBT energy ($hh$-$e_1$) than S2. TE light has no absorption loss in 1550–1640 nm considering ~2 dB waveguide-to-fiber coupling while both TM losses exhibit a broadband ($e_1$-$e_4$). Based on the beam propagation method,[17] the optical confinement factors ($\Gamma$) in CDQW layers are evaluated to be 0.55 for S1 and 0.42 for S2.

Figure 2(a) shows the fiber-based measurement system. A mode-locked fiber laser ($\lambda_1$=1560 nm) was used to excite the $e_1$-$e_4$ transition. A wavelength-tunable semiconductor laser ($\lambda_2$~1.2–1.7 $\mu$m) generated the continuous-wave (cw)

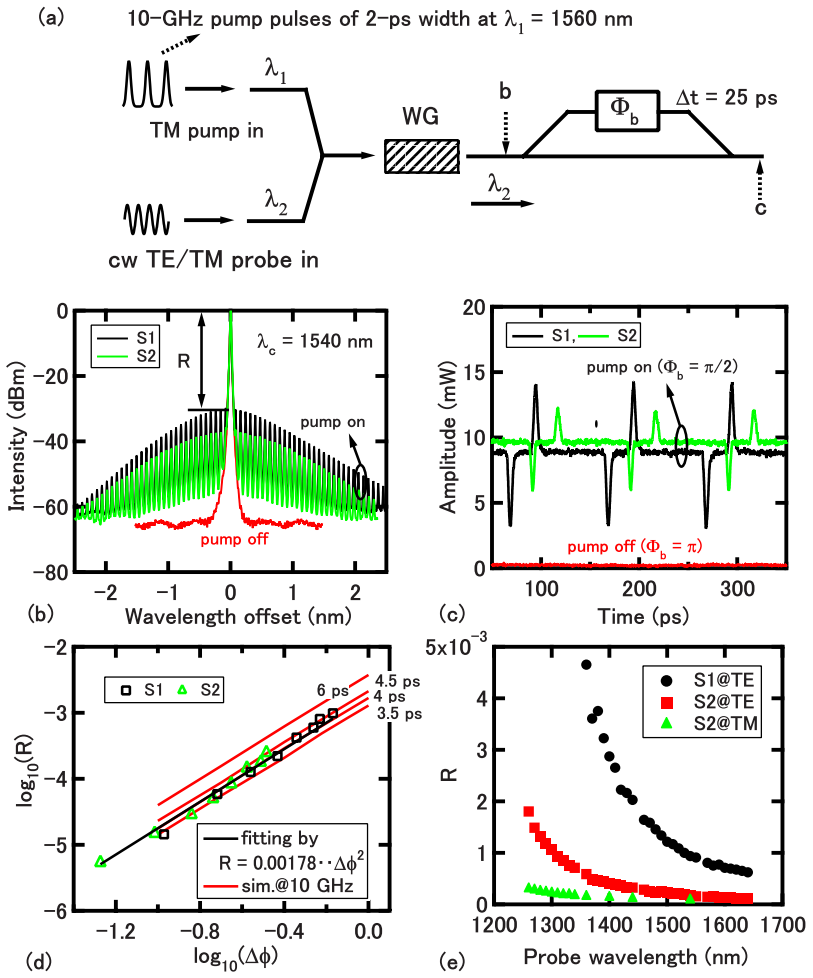


FIG. 2. (Color online) (a) Scheme of the measurement system. The pump wavelength $\lambda_1$=1560 nm. Points *b* and *c*, respectively, indicate the positions for measuring the (b) phase-modulated spectrum and (c) temporal intensity waveform converted from the phase modulation. Both (b) and (c) are measured at $\lambda_2$=1540 nm with the pump energy $E_p$=8 pJ. A ratio *R* is defined and $\Phi_b$ is the phase bias of an interferometer. (d) Comparison of the $R$–$\Delta\phi$ relation between the experiment and the simulation. The FWHMs of phase response are indicated. (e) Wavelength dependent *R* at $E_p$=8 pJ.

probe signal to detect the phase shift $\Delta\phi$. Evaluating $\Delta\phi$ in time domain[7] has a wavelength limit (1530–1565 nm) of the optical sampling scope. In order to overcome this difficulty, we adopt a spectral analysis by measuring phase-modulated spectra [Fig. 2(b)] at point $b$ in which an amplitude ratio $R$ is defined. We intend to derive $\Delta\phi$ from $R$ after calibrating the relation between $R$ and $\Delta\phi$ at $\lambda_2=1540$ nm, where $\Delta\phi$ can be evaluated in time domain [Fig. 2(c)] at point $c$ through an interferometer with a phase bias $\Phi_b=\pi/2$.[7] $\Delta\phi$ in this calibration was adjusted by tuning the pump energy $E_p(<8$ pJ) that refers to the pulse energy inputted into the fiber and meanwhile, for each $\Delta\phi$, we recorded a phase-modulated spectrum to compute the corresponding $R$. Consequently, we can obtain a $R$-$\Delta\phi$ relation at $\lambda_2=1540$ nm and apply this relation to other wavelengths.

In Fig. 2(b), a modulation band occurs under pump since the phase of probe signal is periodically changed whereas it disappears when the pump is off, leaving only a cw component. $\Delta\phi$ increases linearly with $E_p$ with a XPM efficiency slope that is two times higher for S1 (0.088 rad/pJ) than for S2 (0.044 rad/pJ) while $R$ always follows $R\propto E_p^2$ even when tuning the probe wavelength from 1540 to 1360 nm (not shown). Therefore, plotting $R$ versus $\Delta\phi$ at 1540 nm in Fig. 2(d) reveals a sample-independent $R$-$\Delta\phi^2$ relation, i.e., $R$ and $\Delta\phi$ have a one-to-one correspondence.

We have confirmed $R$-$\Delta\phi^2$ by simulating the phase-modulated spectrum through Fourier transforming a cw electrical field $E_x=A\cos(\omega t+\phi)$ with $\phi=\Sigma_j\Delta\phi\exp[-4\ln 2(t-jT_0)^2/t_w^2]$, where $T_0=100$ ps and $t_w$ is the full width at the half maximum (FWHM). As seen in Fig. 2(d), the simulation proves $R$-$\Delta\phi^2$, which can be understood by analytically treating the phase response as a cosine function, as is the case of the widest pulse width.[18] Considering the variations in $t_w$ from 3.7 to 4.2 ps when $E_p$ increases from 1 to 8 pJ, the experimental points are well covered by the simulated lines within $t_w=4\pm0.5$ ps. The width of 4 ps can be convoluted from the pulse width ($\sim$2 ps) by using an exponential decay with an intersubband relaxation time of 2–3 ps that was substantiated by a dynamics study.[19] In addition, $R$-$\Delta\phi^2$ is independent of the probe wavelength.[18] Therefore, it can be used to evaluate the phase shift for other wavelengths.

We measured phase-modulated spectra for TE probe in both samples and TM probe in S2. As shown in Fig. 2(e), $R$ in all three cases increases when shortening the wavelength. This implies a corresponding wavelength dependence of $\Delta\phi$, which obviously contradicts the intersubband plasma model. In particular, the TM light also undergoes a phase shift, presenting another strong evidence to exclude the plasma model. The contrast between S1 and S2 gives us a hint to consider the difference in their $hh$-$e_1$ energies.

Therefore, we propose the interband dispersion model under intersubband excitation in Fig. 3(a). The intersubband excitation pumps a part of the carriers to the excited state $e_4$, and then they relax back to the $e_1$ state by emitting phonons and electron-electron scattering. The Fermi edge experiences a modulation $\Delta E_f$ during this process, which arouses a transient state electron distribution $f_1(E)$. Therefore, the initially blocked IBT becomes allowable within a $k$-space region. The index change ($\Delta n$) will accompany this induced interband

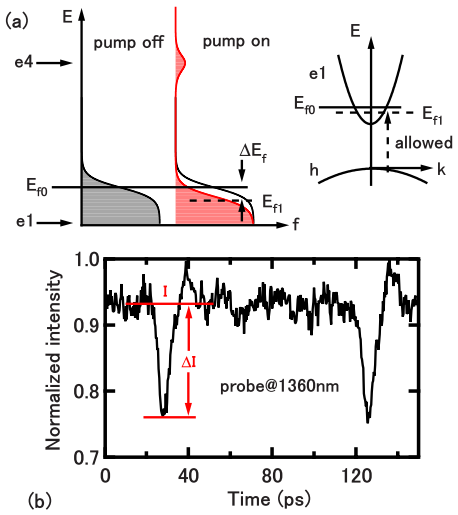


FIG. 3. (Color online) (a) Schematic of the interband absorption enhanced by intersubband excitation. Left: steady [$f_0(E)$ in black shadow] and transient [$f_1(E)$ in red shadow (dark gray line)] electron distribution functions with their corresponding Fermi energies $E_{f0}$ and $E_{f1}$. Right: $E$-$k$ plot revealing a pump-induced interband absorption. (b) Temporal transmission intensity at position $b$ in Fig. 2(a) of the probe light ($\lambda_2=1360$ nm) for S1 under an 8 pJ pump. A length-modified absorption can be defined as $\Delta A=\Delta\alpha L=-\ln(1-\Delta I/I)$. $\Delta\alpha$ is the change in absorption coefficient and $\Delta I$ is corrected by apparatus resolution.

absorption due to their origins in susceptibility[6] and their time responses are clearly determined by the intersubband relaxation process. Therefore, the phase change occurs as $\Delta\phi=\omega\Delta nL/c$, where $L$ is the effective length over which $\Delta n$ is effective and $c$ is the speed of light. In experiment, this induced absorption was observed in Fig. 3(b) where $\Delta A=\Delta\alpha L$ is an analogy with $\Delta\phi\propto\Delta nL$. The wavelength dependence of $\Delta A$ was also measured to be compared with that of $\Delta\phi$. As seen in Fig. 4, $\Delta A$ increases with increasing probe photon energy while S2 has a larger threshold photon energy from which $\Delta A$ obviously starts to increase.

In order to quantitatively explain the wavelength dependent $\Delta A$ and $\Delta\phi$, the interband absorption coefficient $\alpha=(\omega/cn\varepsilon_0)\mathrm{Im}[\varepsilon_0\chi(\omega)]$ can be expressed with a peak absorption coefficient ($\alpha_m$) by assuming a Lorentz-shape spectrum $L(\hbar\omega)$. Then, we can reproduce $\Delta A$ from the difference ($\Delta f$) in electron distribution functions between the steady and transient states by using the product of $L(\hbar\omega)\Delta f$. For a target $\hbar\omega$, we sum this product for all transitions that may contribute to $\Delta A$ as

$$\Delta A=\int_0^\infty \frac{\Gamma M\alpha_m L(\gamma/2)^2}{E_g+E}\cdot\frac{\hbar\omega}{(E_g+E-\hbar\omega)^2+(\gamma/2)^2}\cdot\Delta f\cdot dE, \tag{1}$$

where $E_g$ denotes the IBT energy and $M$ is the period number of quantum wells. Other symbols have their usual meanings. The sum of $E_g$ and $E$ corresponds to the contributive transition energy $E_{\mathrm{ib}}$, and an interband absorption edge $E_0=E_g+E_f$. The effective length $L$ is defined as the length where the pump reaches an intensity attenuation of $1/e$

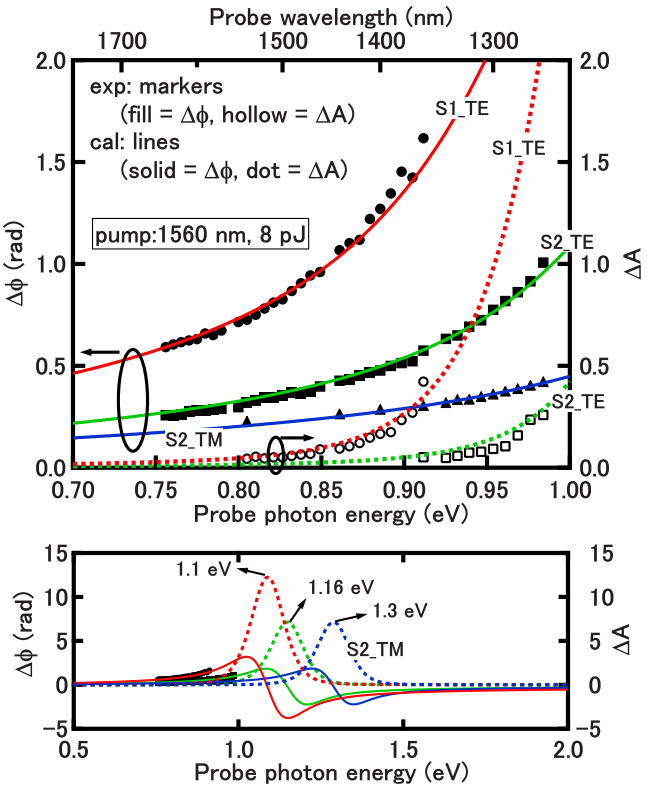


FIG. 4. (Color online) Top: Comparison of the phase shift $\Delta\phi$, and the induced absorption $\Delta A$ between the experiment and the calculation using Eqs. (1) and (2). The experimental $\Delta\phi$ is obtained from Fig. 2(e) using $R=0.00178\ \Delta\phi^2$. Bottom: the whole spectra of $\Delta\phi$ and $\Delta A$. The polarization of probe light is indicated.

($L_{S1}=32\ \mu$m and $L_{S2}=45\ \mu$m). Based on the relation between the absorption coefficient and the refractive index change,[6] the spectrum of the phase shift can be written as

$$\Delta\phi = \int_0^\infty \frac{\Gamma M \alpha_m L(\gamma/2)}{2E_{ib}} \cdot \frac{\hbar\omega(E_{ib}-\hbar\omega)}{(E_{ib}-\hbar\omega)^2+(\gamma/2)^2} \cdot \Delta f \cdot dE. \tag{2}$$

$\Delta A$ and $\Delta\phi$ satisfy Kramers-Kronig transformation, similar to $\Delta\alpha$ and $\Delta n$. If both $\Delta A$ and $\Delta\phi$ have the same origin of interband absorption, Eqs. (1) and (2) will simultaneously predict their spectral features.

In order to calculate $\Delta A$ and $\Delta\phi$ using Eqs. (1) and (2), $E_f$ and $\Delta E_f$ need to be determined first. $E_f$ is $\sim$0.15 and 0.2 eV with $e_1$ as the reference level, respectively, for S1 and S2. In the quantum well plane, the absorption photon number per unit area should agree with the excited carrier density. The sheet density of the absorbed photons is equal to $E_p \cdot 10^{-0.2} \cdot \Gamma \cdot (1-1/e)/(w \cdot L \cdot M \cdot \hbar\omega)$, where $\hbar\omega$ corresponds to the pump wavelength, $E_p=8$ pJ, and mesa width $w=3\ \mu$m. The carrier density changes ($\Delta N$) for S1 and S2 are about $3.6\times10^{11}$ and $2\times10^{11}$ cm$^{-2}$, respectively; these correspond to the average excitation densities of 15% and 6%. Therefore, $\Delta E_f$ is estimated to be about 15 meV for S1 and 8 meV for S2 under the approximation of a two-dimensional electron gas.

Figure 4 compares the experimental $\Delta A$ and $\Delta\phi$, and the calculated ones. For the TE probe at 1640 nm, $\Delta\phi$ of S1 is nearly two times larger than that of S2. Both samples experience a gradual increase in $\Delta\phi$ with increasing photon energy; however, S1 has a larger speed. $\Delta\phi\sim0.5\pi$ is obtained at $\lambda_2=1360$ nm for S1, indicating an XPM efficiency of $\sim$0.2 rad/pJ. This is the largest reported value till now for a nonlinear XPM with a ps-level response in QWs. The calculation using $\alpha_m=7.24\times10^4$ cm$^{-1}$, $E_0=1.1$ eV, $E_g=0.95$, $\gamma=14$ meV, and $\Delta E_f=15$ meV well reproduces both $\Delta A$ and $\Delta\phi$ for S1. The interband absorption coefficient is estimated to be $\sim3.5\times10^4$ cm$^{-1}$ by using Eq. (23) in Ref. 6, supporting that the used $\alpha_m$ is in a reasonable scope. $\gamma=14$ meV implies an interband dephasing time of $\sim$300 fs that depends on temperature and excitation density.[20] For the TE probe in S2, a good agreement is obtained between the experiment and the calculation with $\alpha_m=7.27\times10^4$ cm$^{-1}$, $E_0=1.16$ eV, $E_g=1.01$ eV, $\Delta E_f=8$ meV, and the same other parameters as used for S1. The measured $\Delta A$ for S2 gradually increases when $\hbar\omega>0.9$ eV, as predicted by the calculated line. The two samples have almost the same $\alpha_m$, demonstrating their identical IBT oscillator strength that is usually material independent for the III–V family.[21] Except for the waveguide confinement, $E_0$ is an important parameter in determining the XPM. Compared with S1, S2 has smaller $\Delta\phi$ and $\Delta A$ at the same probe wavelength as well as the slow increase speeds with increasing photon energy because the measured energy region is farther from its $E_0$, as observed in the bottom of Fig. 4. The 60 meV difference in $E_0$ between S1 and S2 is supported by the absorption spectra from which the absorption edge of S2 is estimated to be $\sim$60 meV larger than that of S1. To explain this 60 meV energy, we will calculate the band dispersion by eight-by-eight $k\cdot p$ calculation in future work.

Because of $lh\text{-}e_1 > hh\text{-}e_1$, TM light has a smaller $\Delta\phi$ and a smaller increase speed than TE light. The calculation using $E_0=1.3$ eV and the same other parameters as used for TE light reproduces $\Delta\phi$ for TM light in S2. The 0.14 eV difference in $E_0$ approximately corresponds to the *lh-hh* separation. Therefore, the model in Fig. 3(a) simultaneously explains the wavelength dependent $\Delta\phi$ and $\Delta A$.

To clearly highlight the advantages of our scheme, we give a comparative discussion with another index-modulation scheme: the quantum-confined stark effect, which has been widely used in electro-optical modulators where the external electrical field modulates the interband absorption.[22,23] Generally, the response speed in these modulators is limited by the frequency bandwidth of electrical circuit, typically $\sim$40–100 GHz, which is difficult to reach picosecond level although such an index-modulation magnitude is achievable through conventional quantum stark effect.[23] In our case, we adopt an all-optical means, i.e., intersubband excitation, to induce interband absorption[12–14] that takes place around the Fermi edge when the carriers at the first subband partially depletes. The ps-level intersubband relaxation guarantees the realization of >100 GHz high-speed response in all-optical devices.[8] Such an intersubband pump and interband probe scheme is adopted as a probe technique to study carrier dynamics in Refs. 13 and 14 instead of the nonlinear index change. For telecommunication

applications, both the ISBT and IBT energies should be in the telecommunication wavelength range, which is not achieved in Ref. 12. Such a nonlinear modulation is rarely reported for both ISBT and IBT energies in telecommunication wavelength ranges.

Finally, we check the possible contribution from the plasma effect under the same pump density. The calculation adopts a two-level system with a background index $n_0=3.3$ and an assumed stronger nonparabolicity ($0.06m_0$ and $0.13m_0$ for two levels). $\Delta n=2.1\times10^{-5}$ and $1.3\times10^{-5}$, respectively, for S1 and S2. Then, $\Delta\phi(=2\pi\Delta nLM\Gamma/\lambda)$ at $\lambda=1550$ nm are estimated to be 0.06 and 0.04 rad, both of which are negligible compared with the experiment.

In summary, we confirmed the relation between the phase-modulated spectrum and phase shift, based on which the ultrafast phase shift in QWs was evaluated in the whole telecommunication wavelength range. Tailoring the interband absorption edge to a target photon energy enables us to obtain a great enhancement in XPM. The enhanced interband absorption dominates XPM in photoexcited III–V CDQW waveguides while the intersubband plasma has a negligible contribution.

G. W. Cong acknowledges support from the Japan Society for the Promotion of Science.

*Corresponding author. r-akimoto@aist.go.jp

[1] M. F. Yanik and S. Fan, Phys. Rev. Lett. **92**, 083901 (2004).
[2] P. Dong, S. F. Preble, J. T. Robinson, S. Manipatruni, and M. Lipson, Phys. Rev. Lett. **100**, 033904 (2008).
[3] M. D. Frogley, J. F. Dynes, M. Beck, J. Faist, and C. C. Phillips, Nat. Mater. **5**, 175 (2006).
[4] J. Mørk, T. W. Berg, M. L. Nielsen, and A. V. Uskov, IEICE Trans. Electron. **E87-C**, 1126 (2004).
[5] D. Cotter, R. J. Manning, K. J. Blow, A. D. Ellis, A. E. Kelly, D. Nesset, D. Phillips, A. J. Poustie, and D. C. Rogers, Science **286**, 1523 (1999).
[6] S. L. Chuang and D. Ahn, J. Appl. Phys. **65**, 2822 (1989).
[7] H. Tsuchida, T. Simoyama, H. Ishikawa, T. Mozume, and M. Nagase, Opt. Lett. **32**, 751 (2007).
[8] R. Akimoto, T. Simoyama, H. Tsuchida, S. Namiki, C. G. Lim, M. Nagase, T. Mozume, T. Hasama, and H. Ishikawa, Appl. Phys. Lett. **91**, 221115 (2007).
[9] T. Simoyama, S. Sekiguchi, H. Yoshida, J. Kasai, T. Mozume, and H. Ishikawa, IEEE Photon. Technol. Lett. **19**, 604 (2007).
[10] S. Noda, T. Uemura, T. Yamashita, and A. Sasaki, IEEE J. Quantum Electron. **28**, 493 (1992).
[11] H. Ishikawa, H. Tsuchida, K. S. Abedin, T. Simoyama, T. Mozume, M. Nagase, R. Akimoto, T. Miyazaki, and T. Hasama, Jpn. J. Appl. Phys., Part 2 **46**, L157 (2007).
[12] S. Noda, T. Uemura, T. Yamashita, and A. Sasaki, J. Appl. Phys. **68**, 6529 (1990).
[13] S. Lutgen, R. A. Kaindl, M. Woerner, T. Elsaesser, A. Hase, H. Künzel, M. Gulia, D. Meglio, and P. Lugli, Phys. Rev. Lett. **77**, 3657 (1996).
[14] H. Yoshida, T. Simoyama, A. V. Gopal, J. Kasai, T. Mozume, and H. Ishikawa, IEICE Trans. Electron. **E87-C**, 1134 (2004).
[15] M. Nagase, T. Simoyama, T. Mozume, T. Hasama, and H. Ishikawa, Proceedings of the International Conference on Indium Phosphide and Related Materials (IEEE, Piscataway, NJ, 2007), p. 502.
[16] G. W. Cong, R. Akimoto, K. Akita, T. Hasama, and H. Ishikawa, Appl. Phys. Lett. **90**, 181919 (2007).
[17] G. W. Cong, R. Akimoto, K. Akita, T. Hasama, and H. Ishikawa, Opt. Express **15**, 12123 (2007).
[18] A cw wave with cosine phase modulation can be written as $E(t)=E_0e^{j\omega t}e^{-j\Delta\phi\cos(Ft)}$, where $F$ is the phase modulation frequency. $e^{-j\Delta\phi\cos(Ft)}$ can be expanded using Bessel functions. Then, $R$ between the modulation band and the cw component exactly equals $[J_1(\Delta\phi)/J_0(\Delta\phi)]^2$ ($\propto\Delta\phi^2$ when $\Delta\phi\leq\pi/2$) that is free of the frequency ($\omega$).
[19] C. V.-B. Grimm, M. Priegnitz, S. Winnerl, H. Schneider, and M. Helm, Appl. Phys. Lett. **91**, 191121 (2007).
[20] V. M. Axt and T. Kuhn, Rep. Prog. Phys. **67**, 433 (2004).
[21] G. Bastard, *Wave Mechanics Applied to Semiconductor Heterostructures* (Les éditions de Physique, France, 1992), Chap. 2.
[22] V. Lordi, H. B. Yuen, S. R. Bank, and J. S. Harris, Appl. Phys. Lett. **85**, 902 (2004).
[23] A. Larsson and J. Maserjian, Appl. Phys. Lett. **59**, 1946 (1991).